JOURNAL OF GEOPHYSICAL RESEARCH, VOL. 99, NO. D9, PAGES 18,909–18,921, SEPTEMBER 20, 1994

Effect of changes in radiatively active species upon the lower stratospheric temperatures

V. Ramaswamy and M. M. Bowen

Atmospheric and Oceanic Sciences Program, Princeton University, Princeton, New Jersey

Abstract. A one-dimensional radiative-convective model is employed to investigate the thermal effects in the lower stratosphere due to changes in the concentrations of radiatively active species. In particular, we consider the comparative influences due to species that exert surface-troposphere radiative forcings of opposite signs. Two examples of such competing surface-troposphere forcings are (1) increases in the well-mixed greenhouse gases versus increases in tropospheric aerosols and (2) stratospheric ozone loss versus increase in tropospheric ozone. The radiative equilibrium of the lower stratosphere is perturbed both by the local changes in the concentrations of radiatively active species and by the changes in species' concentrations occurring in the troposphere and the middle/upper stratosphere. Perturbations in the concentrations of each of the species, as considered above, leads to a temperature decrease in the lower stratosphere. Relative to the well-mixed greenhouse gases only case, simultaneous increases in these gases and tropospheric aerosols cause a reduction of the net surface-troposphere radiative forcing, thereby diminishing the surface warming. However, since tropospheric aerosols contribute to a cooling of the lower stratosphere, the temperature decrease there is enhanced above that due to trace gases alone, with the aerosol-induced effects scaling approximately linearly with their optical depth. A complete offset of the greenhouse gas surface-troposphere forcing by tropospheric aerosols, while resulting in a null change in the surface temperature, would double the cooling of the lower stratosphere. Increases in tropospheric ozone would enhance the lower stratospheric cooling over and above that caused by the stratospheric ozone depletion. This is in contrast to the cooling and warming effects exerted upon the surface-troposphere system by the stratospheric and the tropospheric ozone changes, respectively. Tropospheric ozone increases of 20% or more can yield a lower stratospheric cooling that is a significant fraction of the effects due to the observed stratospheric ozone loss. Both the surface effects and the enhancement of the lower stratospheric cooling scale approximately linearly with tropospheric ozone increases.

1. Introduction

It has been realized recently that over the past century or more, the climate of the surface-atmosphere system has been forced not only by the radiative effects of the well-documented increases in the concentrations of the uniformly mixed anthropogenic greenhouse gases or GHGs (CO_2, CH_4, N_2O, and chlorofluorocarbons (CFCs)) but also possibly by the effects due to an increase in the anthropogenic component of tropospheric aerosols [*Charlson et al.*, 1991, 1992; *Penner et al.*, 1992]. Since the surface-troposphere forcing by tropospheric aerosols is opposite to that for the greenhouse gases [*Intergovernmental Panel on Climate Change (IPCC)*, 1992], this gives rise to the notion of competing forcings' having been in operation over the past century. The IPCC scientific assessment also presents a second potential scenario of competing radiative forcings that may have existed over the past decade or so, namely, the decrease in lower stratospheric ozone, which causes a negative radiative forcing of the surface-troposphere system, versus the increase in tropospheric ozone, which yields a positive forcing (see also *World Meteorological Organization (WMO)* [1992]). Both of these examples from the recent state-of-the-art scientific assessments conjure up a more intricate portrait of the net radiative forcing of the global climate system than that obtained when only the well-mixed greenhouse gases are considered.

An estimate of the global surface temperature change resulting from trace gas and aerosol radiative forcings can be obtained using a one-dimensional radiative-convective model (1-D RCM). From the definition of the surface-troposphere radiative forcing and the known characteristics of RCMs [*WMO*, 1986] the net effect due to two forcings of opposite signs can be expected to change the surface temperature less than either one acting alone. For example, tropospheric sulfate aerosol increases would mitigate the surface warming resulting from greenhouse gas increases. However, while such a qualitative understanding of the influences on the surface temperature due to simultaneous increases in trace gas and aerosol increases is readily obtained, an intriguing and unanswered aspect is the accompanying effects in the stratosphere, particularly the lower stratosphere.

In the problem involving atmospheric ozone changes, a negative radiative forcing of the surface-troposphere system

Paper number 94JD01310.
0148-0227/94/94JD-01310$05.00

due to the observed stratospheric losses [*Ramaswamy et al.*, 1992] can be offset by simultaneous increases in tropospheric ozone [*Lacis et al.*, 1990; *Schwarzkopf and Ramaswamy*, 1993; *Wang et al.*, 1993]. Again, while this may result in a small net impact within the surface-troposphere system, a question of interest is the consequence in the lower stratosphere due to the presence of these competing forcings.

We address the issue posed above using a modified version of the globally and annually averaged 1-D RCM described by *Ramaswamy and Kiehl* [1985] (hereinafter referred to as RK). Two separate studies are conducted to investigate the mechanisms governing the radiative fluxes and the thermal response of the lower stratosphere due to surface-troposphere radiative forcings of opposite signs. First, we study the relative effects of the increases in well-mixed greenhouse gases and tropospheric aerosols, as well as the effects due to simultaneous increases in both of these species. Second, we examine the effects due to stratospheric ozone decreases and the additional influences due to different amounts of tropospheric ozone increases. The investigation consists of analyzing the changes in the radiative fluxes and heating rates and the changes in the atmospheric thermal profile.

2. Model Description

The 1-D RCM has 28 layers (surface to 50 km), and its basic physics is similar to that given by RK. The longwave transfer scheme is identical to that of RK, but the solar fluxes and heating rates are computed differently; the new method is described in the Appendix. The solar spectrum is divided into 56 distinct spectral bands while the longwave spectrum comprises 18 bands. Solar spectral insolation at the top of the atmosphere follows *Labs and Neckel* [1970]. The cosine of the mean zenith angle and the fraction of day are each assumed to be 0.5.

The model accounts for the radiative effects due to CO_2, O_3, H_2O, CH_4, N_2O, chlorofluorocarbons F-11 and F-12, Rayleigh scatterers, aerosols, and clouds. The computation of the radiative properties of the gaseous species in each layer remains the same as in the work of RK. For the GHG increases we consider the changes in the concentrations of CO_2, CH_4, N_2O, F-11, and F- from 1850 to the end of the 1980s. For 1850 the concentrations adopted are as listed by *WMO* [1986]. We use the 1988 concentrations as representative of the end of the past decade. The 1988 values are obtained using the growth formulations given by *Ramanathan et al.* [1985] for CO_2 and by *WMO* [1986] for the rest of the GHGs. The vertical profile of O_3 follows that of *Ramanathan and Dickinson* [1979]. This profile is perturbed in the experiments involving changes in atmospheric ozone. The water vapor profile below ~14 km is obtained using the prescription of *Manabe and Wetherald* [1967], assuming a fixed surface relative humidity of 77%. Above this altitude, the water vapor mixing ratio is fixed at 3 parts per million by mass (ppmm).

The present model employs a random overlap of three clouds situated between 1.6 and 3, 4.2 and 5.6, and 9.2 and 10.4 km, respectively. The cloud amounts assumed are 0.33 for high, 0.08 for middle, and 0.23 for low clouds; these values are typical of those employed in 1-D RCMs [*Manabe and Wetherald*, 1967; *Ramanathan*, 1981]. Emissivities of the low and middle clouds are assumed to be unity while that for the high cloud is 0.5. The single-scattering albedo and the asymmetry factor for all three clouds in the solar spectrum assume the same values as for the cloud in RK. The extinction optical depth in the visible spectrum is assigned values of 4, 10, and 13.6 for the high, middle, and low clouds, respectively. The values of the cloud parameters chosen for this study are arbitrary but yield a reasonable simulation of the unperturbed temperature profile.

The optical properties of aerosols in the visible follow the *Coakley et al.* [1983] parameterization for the 70% tropospheric aerosol model of *Shettle and Fenn* [1979]. The near-infrared single-scattering properties and the terrestrial infrared absorption properties are adapted directly from *Shettle and Fenn* [1979]. The distribution of aerosol concentrations in the vertical follows the "clear atmosphere" model of *McClatchey et al.* [1972]. Changes in tropospheric aerosol optical depth are simulated by varying the concentrations at all altitudes below ~14 km by the same factor.

The radiative-convective model parameterizes convection with a Fickian diffusion scheme as discussed by RK and uses the same parametric values. The model has a "swamp" surface with zero heat capacity. The surface temperature is solved using an explicit energy balance equation. Radiative-convective equilibrium is assumed to be established when the total (net radiative plus convective) flux across each level is less than 0.005 W m^{-2}. The model is used in both radiative and radiative-convective modes. In the radiative mode the 1-D model is used to determine the instantaneous changes in the longwave and solar fluxes and heating rates caused by a perturbation of specific atmospheric constituents, keeping all other parameters fixed. In the radiative-convective mode the effects due to changes in the constituents on the equilibrium temperature profile are investigated by allowing the model to reach a new radiative-convective equilibrium. In this study we choose the 16-km level as the tropopause; this is within 1 km of the minimum occurring in the temperature profile.

3. General Radiative Considerations

For the purposes of this study we focus on the 16- to 23-km region in the model and refer to it as the lower stratospheric region. The globally and annually averaged stratosphere tends to be in radiative equilibrium, with the solar heating being balanced by the longwave cooling. The lower stratospheric radiative heating and cooling rates generally tend to be small in magnitude [*Manabe and Moller*, 1961; *Kiehl and Solomon*, 1986], but the radiative damping rates tend to be large [*Fels*, 1982]. Both the cool-to-space mechanism and the exchange with the underlying and the overlying portions of the atmosphere contribute to the net radiative heating in this region [*Rodgers and Walshaw*, 1966].

Perturbations to the solar and the longwave fluxes in the lower stratosphere can be brought about by changes in the local concentrations of radiatively active species. For example, local perturbations to the fluxes occur in the case of greenhouse gas increases and ozone decreases in the lower stratosphere [*WMO*, 1986, 1992] which, in turn, alter the absorption and emission properties of that region. Perturbations to the flux at the boundaries of the lower stratosphere can also affect the radiative balance of the region. The upwelling longwave flux at the base of the lower stratosphere

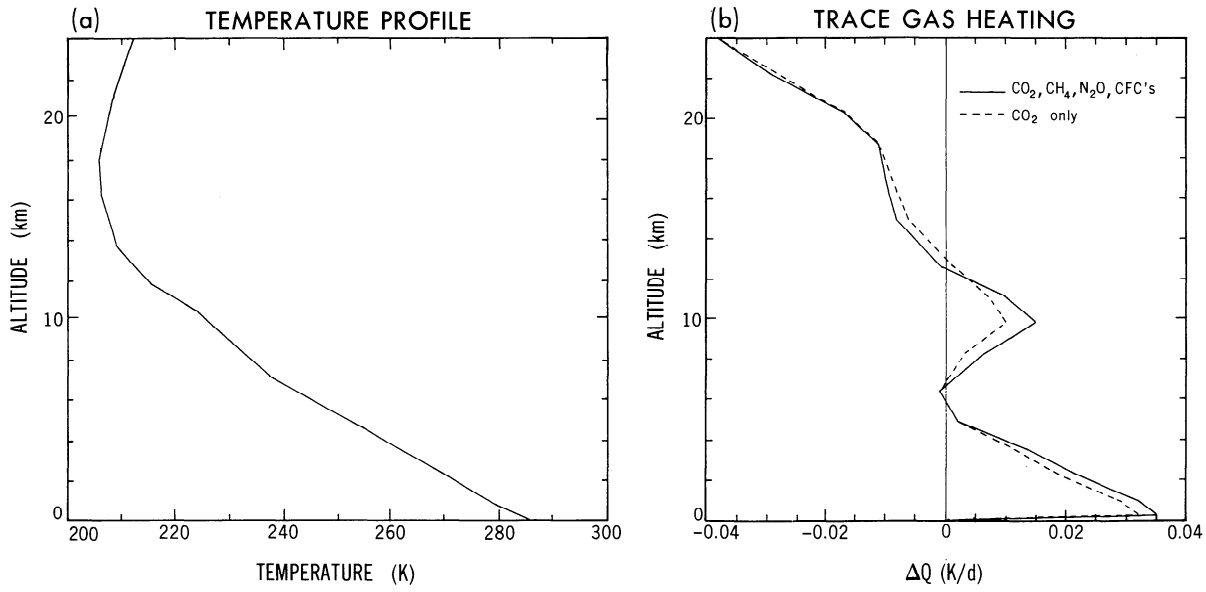

Figure 1. (a) Vertical profile of the equilibrium temperature obtained using the one-dimensional RCM and the well-mixed greenhouse gas (CO_2, CH_4, N_2O, F-11 and F-12) concentrations corresponding to the year 1850 and (b) change in the radiative cooling rates due to increases in the gases between 1850 and 1988 (see section 4.1). The change due to an increase in CO_2 only is also shown.

is influenced both by variations in tropospheric temperature and by the concentrations of radiatively active species in the troposphere such as CO_2, H_2O, and O_3. For example, an increase in the concentration of an infrared active gas in the troposphere, keeping all other parameters fixed, would tend to reduce the upwelling longwave flux at the tropopause [*WMO*, 1986]. On the other hand, a warmer troposphere, keeping all other parameters fixed, would result in an increase of the upwelling flux by virtue of increased tropospheric emission.

The downwelling longwave flux at 23 km, arising because of emission from the upper and middle stratosphere, is influenced by changes in the concentrations and the temperatures in that region. This downward longwave stream also affects the flux convergence within the lower stratosphere. However, the influence of the upper stratosphere (say, above 35 km) on the atmospheric regions below becomes less with increasing altitude, owing to the accompanying increase in infrared opacity between the two regions [*Ramanathan et al.*, 1985].

Any change in the flux convergence within the lower stratosphere due to any or all of the reasons stated above leads to a perturbation in the temperature there. This tends to further alter the emission from the lower stratosphere and affects the fluxes emerging from the 16- to 23-km layer. Ultimately, a new radiative equilibrium is established in the lower stratosphere, which involves changes in the local temperature [*Fels et al.*, 1980].

In the following text we examine the changes induced in the 16- to 23-km region with respect to an initial radiative-convective equilibrium (RCE) state. Both the changes corresponding to the instantaneous perturbation (i.e., due to a change solely in species concentration) and the final RCE state are discussed. Besides the changes in the thermal profile, we also analyze the changes in the lower stratospheric radiative energy balance by considering specifically the net solar, the upward longwave, and the downward longwave fluxes at 16 and 23 km and the convergence or divergence in these fluxes across the 16- to 23-km region. As a point of reference, Figure 1a illustrates the RCE thermal profile from zero to 24 km, obtained using the 1850 trace gas concentrations with no aerosols. In this state the solar convergence across the 16- to 23-km layer is 1.77 W m^{-2}, which is balanced by a longwave divergence of an equal but opposite amount. The net longwave effect comprises a divergence in the downward longwave flux of −4.17 W m^{-2} and a convergence in the upward longwave flux of 2.4 W m^{-2}.

4. Well-Mixed Greenhouse Gases and Tropospheric Aerosols

4.1. Initial Radiative Perturbations

Corresponding to the RCE thermal profile in Figure 1a, Figure 1b shows the instantaneous change in the heating rate due to the increases in the concentrations of the well-mixed greenhouse gases between 1850 and 1988, with temperature, water vapor, and ozone held fixed. Only the troposphere and the lower stratospheric regions are emphasized. The result due to considering only the CO_2 increase is also shown in Figure 1b, and its leading role in the perturbation is apparent. The radiative heating perturbation consists of the tropospheric warming tendency caused by the increases in the infrared absorbers [*WMO*, 1986]. It decreases with height until about ~6 km, then increases until ~10 km. Above 10 km there is a decrease, with an increasing cooling tendency with altitude above ~13 km. The location of the upper tropospheric altitude where the transition occurs from a warming to a cooling perturbation is very sensitive to the assumed temperature and moisture distributions. The heating due to the inclusion of the non-CO_2 gases results in an increased warming over that due to CO_2 in the troposphere, along with a slightly increased cooling in the lower strato-

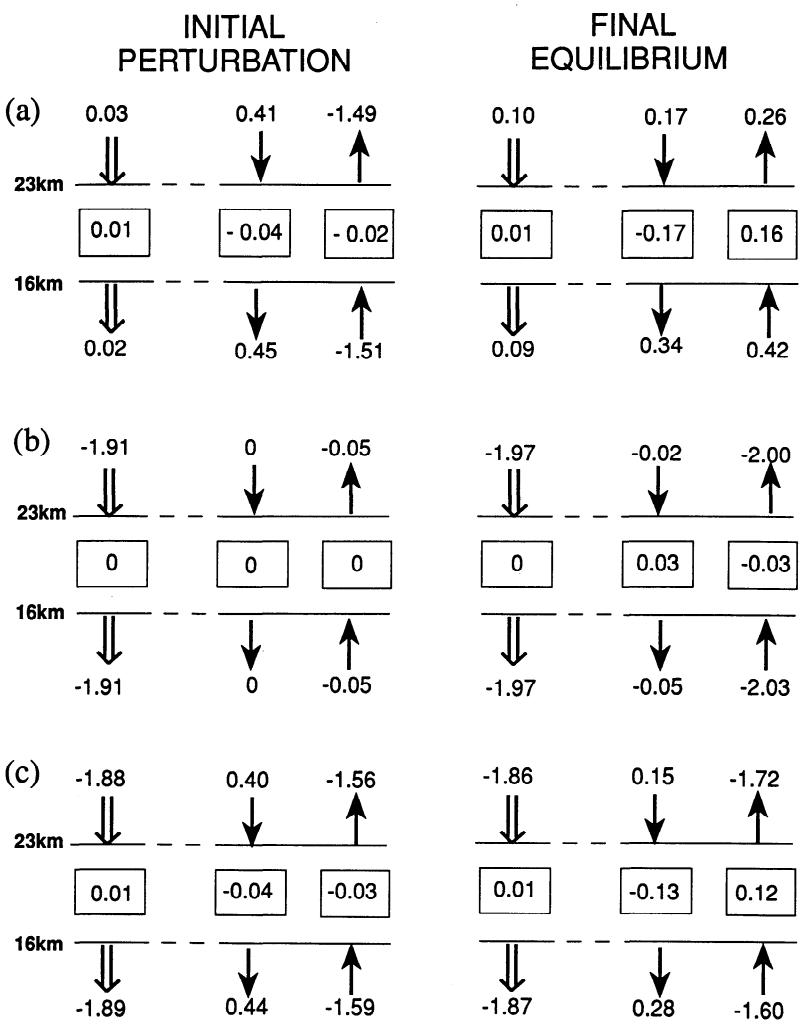

Figure 2. Change in the net solar (open arrow) and upward and downward longwave (solid arrows) fluxes (watts per square meter) at 16 and 23 km and the respective flux convergences (boxed values) within the 16- to 23-km layer corresponding to (a) trace gas increases only (1850–1988), (b) tropospheric aerosol optical depth increase from zero to 0.066, and (c) combined trace gas and aerosol effects (see section 4). All the changes are with respect to the values at the initial radiative-convective equilibrium state corresponding to 1850 concentrations of CO_2, CH_4, N_2O, F-11 and F-12, and with no aerosols. For reference the values at the initial equilibrium for the flux convergences within the 16- to 23-km layer are 1.77 (solar), −4.17 (downward longwave), and 2.4 (upward longwave) W m^{-2}. (Left) The initial perturbations due to changes in the concentrations only and (right) the changes corresponding to the final radiative-convective equilibrium state (see section 4) are represented.

sphere. The surface-troposphere forcing (i.e., the net radiative flux change at the model tropopause) for the GHG increases is 1.97 W m^{-2}, approximately similar to the value of 2.04 W m^{-2} obtained by *Hansen and Lacis* [1990].

The initial perturbations to the cloudy sky fluxes at 23 and 16 km and to the net flux convergences within the region bounded by these levels are illustrated in Figure 2a (left). The increase in the tropospheric absorber concentrations, particularly CO_2, and the resulting changes in the CO_2-H_2O overlap effects [*WMO*, 1986] cause a decrease in the upwelling longwave flux. On the other hand, the increase of CO_2 in the upper stratosphere leads to an enhancement of the downwelling flux at 23 km. The increase of absorber amount in the 16- to 23-km region enhances the emission from this layer. The net effect in the 16- to 23-km layer is an increase in the divergence (i.e., loss of energy) of the downward longwave and a reduction in the convergence (also an energy loss) of the upward longwave beams. Considering also the increase in the net solar convergence due to CO_2, the initial net radiative perturbation in the lower stratosphere is a flux divergence and yields a cooling tendency, as manifested in Figure 1b.

Considering tropospheric aerosols next, we employ the model described in section 2 to simulate the forcing due to increases in tropospheric aerosol optical depth. In order to highlight the nature of the forcing and its effects, we consider a specific but deliberate perturbation in the tropospheric aerosol optical depth. The aerosol optical depth value chosen is 0.066; this yields a surface-troposphere forcing that is similar in magnitude but opposite in sign to the trace gas effect (−1.95 W m^{-2}). The initial flux changes that arise in the 16- to 23-km region, again holding temperatures and

moisture fixed, are shown in Figure 2b (left). There is no change in the 16- to 23-km layer flux convergence/divergence due to the net solar flux, the downward longwave flux, or the upward longwave flux; this is because of the absence of a change in any radiatively active constituent in this region. There is a reduction in the upward longwave flux, the magnitude of which is uniform throughout the lower stratosphere. This reduction is due to the tropospheric aerosol infrared opacity's behaving much like that for a "greenhouse" gas. There is also a reduction in the net downward solar flux, which is uniform throughout the stratosphere. This is due to the enhanced reflection by the aerosols which reduces the solar flux absorbed by the surface-atmosphere system. Thus the aerosol-induced change in tropospheric opacity has a negligible initial effect on the lower stratospheric flux convergence. The same characteristics hold for the middle and upper stratosphere, too, so that there is virtually no initial aerosol-induced solar or longwave perturbation throughout the stratosphere.

Applying GHG and tropospheric aerosol increases simultaneously results in an initial perturbation of the lower stratosphere that is an approximate sum of the two individual effects, as can be seen by comparing Figure 2c with Figures 2a and 2b. This is true for the fluxes at the 16- and the 23-km levels as well as for the changes in the convergence/divergence of fluxes within this layer.

4.2. RCM Equilibrium Results

The changes between the final and the initial equilibrium temperature profiles are illustrated in Figure 3a for all the three cases considered above. It is noted that in this figure, it is the surface-air rather than the surface value that is distinguishable. The GHGs' increase exhibits the well-known temperature increase in the troposphere and a temperature decrease in the stratosphere [*WMO*, 1986]. The surface-air temperature increase is approximately 1 K. The temperature decrease above 30 km is almost entirely due to the increase in CO_2 concentrations. The discontinuous nature of the curve is in part due to the model vertical resolution and the convective parameterization employed. The changes in the lower stratosphere fluxes at the new RCE state, relative to the corresponding quantities at the initial equilibrium, are shown in Figures 2a, 2b, and 2c (right) for all three cases discussed in the previous section.

By comparing the flux changes at the final RCE state and that during the initial perturbation (i.e., left and right panels of Figure 2a), we examine the adjustment in the fluxes due to changes in the atmospheric thermal profile. In the case of the GHGs the tendencies shown in Figures 1b and 2a cause a decrease of the temperature in the middle and upper stratosphere which leads to less of an increase (compared to the initial perturbation) in the downward longwave flux at 23 km. Simultaneously, the lower stratosphere cools, reducing its emission. The net result of these two effects is a further increase (compared to the initial tendency) in the divergence of the downward longwave beam. The tropospheric warming tendency indicated by Figure 1b leads to an increase in the tropospheric temperatures (Figure 3a); this results now in an enhancement of the upward longwave flux at 16 km. Combined with the cooling of the lower stratosphere, the result at equilibrium is an increase in the convergence of the upward longwave beam. In the new RCE state the changes in the flux convergence for the two longwave components together

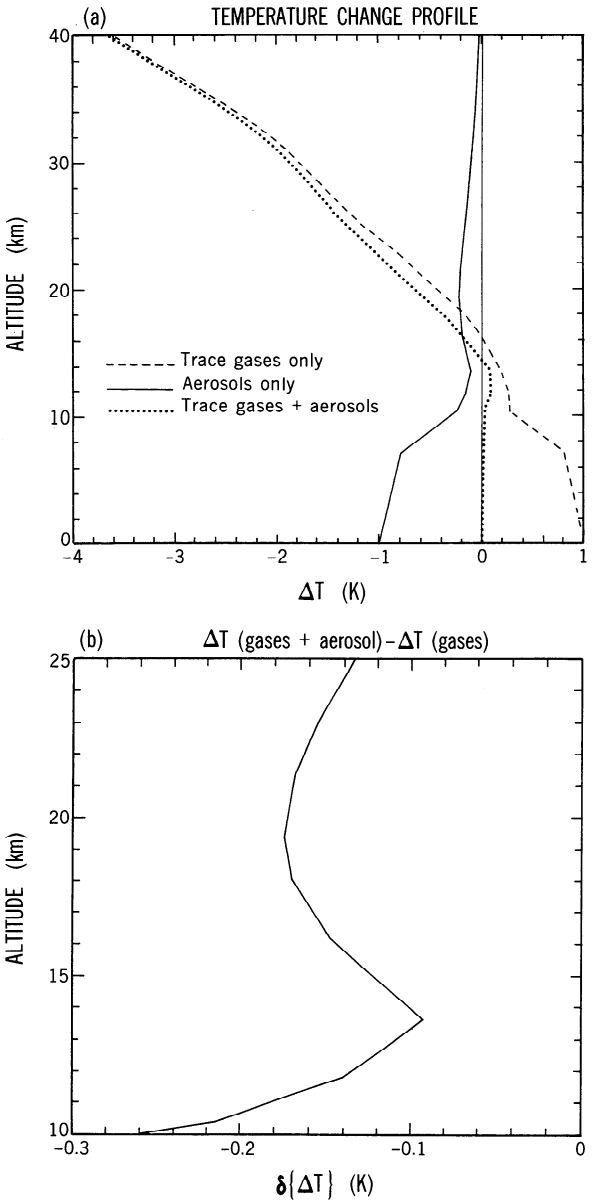

Figure 3. (a) Vertical profile of the change in temperature (ΔT) due to trace gas increases only, aerosol increases only corresponding to an optical depth of 0.066, and a simultaneous increase in both gases and aerosols and (b) change in temperature $\delta\{\Delta T\}$ between the gas plus aerosol case and the gas only case in the altitude range 10–25 km (see section 4.2).

again balance the increase in the solar flux convergence. It is of interest to note that in both the initial and the final RCE states, the magnitude of each longwave convergence component exceeds the net solar value.

Consider next the case of aerosol increase only (left and right panels of Figure 2b). In this case the troposphere cools (see Figure 3a) in response to the increase in its albedo. Because of the near equivalence of the magnitudes of the initial radiative forcing, the surface and tropospheric temperature changes due to the GHGs and the aerosol increases are nearly similar in magnitude but have opposite signs. The tropospheric cooling is accompanied by a reduction of the upward longwave flux at 16 km. Compared with the value for the instantaneous perturbation, there is a substantial change

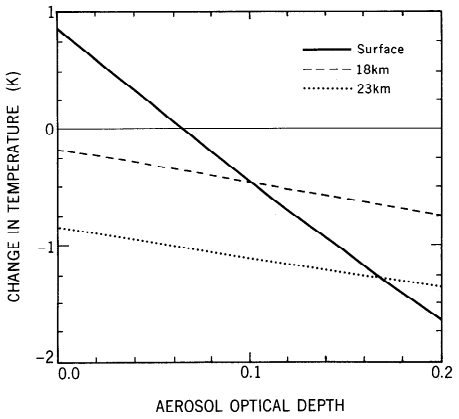

Figure 4. Change in temperature at surface, 18 km, and 23 km due to a simultaneous change in trace gas concentrations (corresponding to the 1850–1988 increases) and tropospheric aerosols, as a function of aerosol optical depth (see section 4.2).

in the upward longwave flux. The magnitude of the change in the upward flux, in going from the initial perturbation to the final RCE state, is approximately similar ($\sim$2 W m^{-2}) to the trace gas case but in the opposite sense. The stratosphere also cools (Figure 3a), reducing its emission. The simultaneous cooling of the lower stratosphere and the troposphere is such that there is a reduction in the flux convergence of the upward longwave beam within the 16- to 23-km region at the new equilibrium; this is in contrast to the gas-only case where there is an increase (Figure 2a). The slight cooling of the middle stratosphere is accompanied by slightly less downward flux at 23 km and a slight decrease in the divergence of this component within the lower stratosphere; this, too, is in contrast to the changes for the gas-only case. Figures 2a and 2b indicate that there is a distinct difference in the manner in which the longwave radiative components react in reestablishing radiative equilibrium in the lower stratosphere for the GHGs and the aerosol changes, respectively.

As with the issue of the initial perturbation, the case with simultaneous increases in aerosol and GHG concentrations exhibits flux and temperature changes at equilibrium that are approximately a sum of the two individual cases discussed above (Figure 2c (right) and Figure 3a). In the troposphere the two equal but opposite forcings cancel, resulting in a near-zero temperature change from the surface up to near the tropopause. Above $\sim$15 km the pattern resembles the GHGs-only case although the temperature changes, influenced by the additional presence of the tropospheric aerosols, are now greater in magnitude.

Figure 3b highlights the difference in the temperature response $\delta\{\Delta T\}$ between the GHGs plus aerosol and the GHGs-only case in the 10- to 25-km region. It demonstrates the sensitivity of the lower stratospheric thermal profile to the influence of tropospheric aerosols. The tropospheric aerosol cools the stratosphere by approximately 0.08–0.26 K more than the GHG increases alone. Thus an important inference is that although the tropospheric aerosol forcing may completely offset the GHG effects at the surface and in the troposphere, it enhances the trace gas cooling in the lower stratosphere. At 18 km the change due to the trace gases only is -0.18 K; with aerosols included, the additional change is -0.18 K, a 100% increase in the cooling. At 23 km, GHGs alone yield a larger change (-0.86 K); the additional cooling due to the aerosols is $\sim$20%. The radiative influence of troposphere at 23 km is less than that at 18 km owing to the increasing infrared opacity and therefore the decreasing importance of the longwave exchange processes with the underlying atmosphere as altitude increases. Still higher up, the differences due to tropospheric aerosols become even less, and the middle and upper stratosphere temperature decreases for the GHGs plus aerosol case are virtually identical to that for the GHGs-only case. There is little additional change in the temperature above 35 km.

The physical mechanism described above for the effects in the lower stratosphere holds true for other tropospheric aerosol optical depths as well. In order to discern the temperature effects at different aerosol optical depths, we have performed RCE experiments in which the GHGs' perturbation corresponds to the 1850–1988 changes, while the tropospheric aerosol optical depth perturbation is increased through a range of values from zero to 0.2. Over this range the aerosol layer corresponds approximately to the thin optical depth limit in the visible spectrum. Figure 4 shows the resulting temperature changes obtained at the surface, at 18 km, and at 23 km as a function of aerosol optical depth and indicates that the aerosol-induced effects scale almost linearly with the optical depth perturbations considered. Table 1 lists the rate of temperature change at the three altitudes.

In the absence of an aerosol perturbation the surface temperature change is $\sim$0.85 K (see Figure 3a for the corresponding surface-air temperature change), in approximate agreement with expectations from 1-D RCM sensitivities [*WMO*, 1986]. As aerosol optical depth increases, there is a diminution of the GHGs' warming effect, and there results a decrease in the net change in the surface temperature ($\sim$1.27 K per 0.1 increase in optical depth). At an optical depth of approximately 0.066, as discussed above, the aerosol counteracts completely the forcing due to the GHG increases, and the surface temperature change is nearly zero. For optical depths exceeding $\sim$0.066 the aerosol forcing dominates, and the net GHGs plus aerosol effect is one of a surface cooling. It is noted that the precise value of the optical depth that would offset some specific greenhouse gas effect would differ for different aerosol models.

At 18 km there is a cooling (-0.18 K) in the absence of aerosol changes, as already discussed. The lower stratospheric cooling increases with aerosol optical depth, and

Table 1. Rate of Change of Temperature at the Surface and in the Lower Stratosphere When Simultaneous Increases in Well-Mixed Greenhouse Gas Concentrations (1850–1988) and Tropospheric Aerosols Are Considered

	Rate of Change
Surface	-1.27 K per 0.1 increase in tropospheric aerosol optical depth
18 km	-0.29 K per 0.1 increase in tropospheric aerosol optical depth
23 km	-0.26 K per 0.1 increase in tropospheric aerosol optical depth

See section 4 and Figure 4.

there are circumstances when the magnitude of this temperature change can exceed that at the surface. The rate of temperature change at 18 km is −0.29 K per 0.1 increase in optical depth over the range of optical depths considered here. At 23 km, too, the cooling effect increases with optical depth. The rate of change at 23 km is slightly less than that at 18 km (−0.26 K per 0.1 increase in optical depth). In general, as optical depth increases, temperatures decrease at all altitudes in the atmosphere.

We now comment on the potential effects due to tropospheric aerosols over the past century using the results from the present aerosol model (Figure 4) and some recent radiative-forcing estimates. The global surface-troposphere radiative forcing due to an increase in the anthropogenic component of the sulfate aerosol was estimated by *Charlson et al.* [1991] as -0.6 W m^{-2}, with an uncertainty of a factor of 2. In the work of *Charlson et al.* [1992] the mean value is inferred to be -1 W m^{-2}. *Kiehl and Briegleb* [1993], using a more detailed radiative transfer model, infer a global mean value of about -0.3 W m^{-2}. *Penner et al.* [1992] estimate a forcing of -1 W m^{-2} for the increase due to aerosols from biomass burning (again with an uncertainty of a factor of 2), although this value could be an overestimate [*Kiehl and Briegleb*, 1993]. Thus the estimated global surface-troposphere forcing, at least for the aerosol components postulated to have increased since 1850, suggests a mean value ranging from 0.3 to 2 W m^{-2}; the higher limit would imply a nearly complete offset of the GHGs' forcing to date.

As examples, we consider forcings of 0.3, 0.6, 1, and 2 W m^{-2}, which would correspond to optical depths of $\sim 1.0 \times 10^{-2}$, 2.0×10^{-2}, 3.3×10^{-2}, and 6.6×10^{-2}, respectively, in the context of the present aerosol model. From Figure 4 the surface temperature reduction brought about by these optical depths, as a percentage of the total greenhouse gas effect, would be 15, 29, 49, and 99%, respectively. At 18 km the additional cooling contribution by the aerosols, relative to that due to GHGs, would be 18, 36, 60, and 100%, respectively. And at 23 km the additional cooling induced would be 3, 6, 10, and 20%, respectively. Thus if the global forcing by tropospheric aerosols over the past century has been >0.6 W m^{-2}, the additional lower stratosphere cooling would be a significant fraction of the GHG effects. If aerosol optical depths continue to increase, Figure 4 suggests that the aerosol-induced cooling would become comparable to or even exceed the GHG effects. Although this discussion is based on a specific aerosol model and more precise estimates must await details on the actual changes that have occurred or are occurring for different types of aerosols, the physical mechanism discussed would hold true in a general sense.

5. Atmospheric Ozone

In this section we examine the surface-troposphere radiative forcings in the context of ozone changes in the atmosphere. Observations [*WMO*, 1992] have now established that there has been a global loss of ozone in the lower stratosphere during the decade of the 1980s. At the same time and perhaps extending over the past two decades, some locations in the northern hemisphere midlatitudes suggest an increase in tropospheric ozone. The stratospheric and the tropospheric ozone changes arise because of entirely different chemical processes [*WMO*, 1992].

We investigate the effects due to stratospheric ozone change by considering the vertical profile of the mean ozone loss above ~10 km, as given by *Miller et al.* [1992, Figure 1]. This profile is based on an average from several ozonesonde measurements up to about the mid-1980s and shows the peak percentage loss (7%) to be at ~20 km. The mean percentage loss decreases with decreasing altitude; between ~15 and 10 km these values become progressively small and may not be statistically significant. In fact, details of the profile of ozone changes from the upper troposphere and into the lowest portions of the lower stratosphere are somewhat uncertain [*WMO*, 1992], and this could have a significant bearing on the forcing [*Schwarzkopf and Ramaswamy*, 1993]. The column ozone loss in the model as a result of applying the depletion profile is 6 Dobson units (DU). We investigate the additional effects due to increases in tropospheric ozone by assuming uniform percentage increases in the model ozone below 10 km. The assumptions about the distribution of ozone changes in the stratosphere and the troposphere (including the amount of change), although critical for a precise quantitative assessment of the climate changes, have a simple form here, with the aim being to highlight the physical mechanisms in play. We consider in particular a 10 and a 20% increase in tropospheric ozone. The 10% value is representative of decadal trends from some ozonesonde measurements over approximately the past two decades [*WMO*, 1992]. The 20% decadal change is typical of the largest reported (e.g., Hohenpeissenberg, Payerne) measurements but likely represents the trend only over very polluted regions in the northern hemisphere midlatitudes. In the current model the 10 and the 20% increases yield column ozone gains of ~2 and 4 DU, respectively.

5.1. Initial Radiative Perturbations

As in the trace gas–aerosol case, radiative calculations are performed to investigate the instantaneous change in the heating rates produced by a decrease of stratospheric ozone and an increase of tropospheric ozone, with the temperature and the concentration of the other species held fixed. The initial equilibrium temperature profile adopted (not shown) is that obtained from the one-dimensional RCM corresponding to the 1988 concentrations of CO_2, CH_4, N_2O, and CFCs and with no aerosols. This result is virtually indistinguishable from that shown in Figure 1a. Figures 5a, 5b, and 5c show the solar, longwave, and net heating rates, respectively. In each panel the results corresponding to a fixed stratospheric loss but with a 0%, 10%, and 20% increase of tropospheric ozone, respectively, are illustrated. The initial changes in the flux dispositions are displayed for the stratospheric loss case only (Figure 6a, left) and for the case with the 20% tropospheric increase (Figure 6b, left). It is pointed out that as a consequence of the different initial RCE state assumed here, the numerical reference values for the 16- to 23-km fluxes differ from those in section 3; the focus will be on the departures from the reference values.

The instantaneous solar heating rate perturbation (Figure 5a) is dominated by a marked decrease in the lower stratosphere, peaking at ~20 km. The loss of ozone in the lower stratosphere leads to less photon absorption there [*Fels et al.*, 1980] and more absorption below the 16- to 23-km layer (Figure 6a). The solar perturbations in the stratosphere or the troposphere are hardly affected by the tropospheric ozone increases; the effects are barely distinguishable in the lower troposphere.

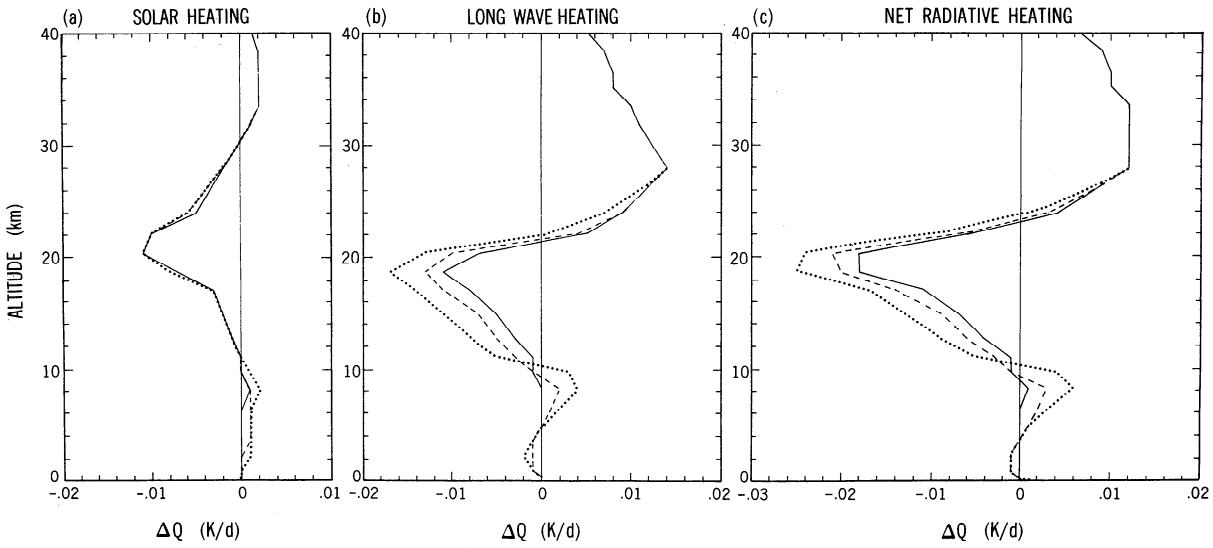

Figure 5. Change in the instantaneous (a) solar, (b) longwave, and (c) net radiative heating rates due to a decrease in stratospheric ozone. The changes for stratospheric loss only (solid curve) and the changes for 10% (dashed curve) and 20% (dotted curve) increases in tropospheric ozone are also considered (see section 5.1).

Figure 5b illustrates the changes in the longwave heating rates. We note first that the radiative transfer in the 9.6-μm ozone band yields a heating in the lower stratosphere, with cooling above ~27 km [see *Schwarzkopf and Fels*, 1991, Figure 26]. The loss of stratospheric ozone yields a cooling tendency in the lower stratosphere, with a peak at ~19.5 km and decreasing below. Above this height the cooling decreases while from ~21 to 40 km there is a heating perturbation. These effects are due to the perturbation in the 9.6-μm radiative transfer arising as a result of the loss of

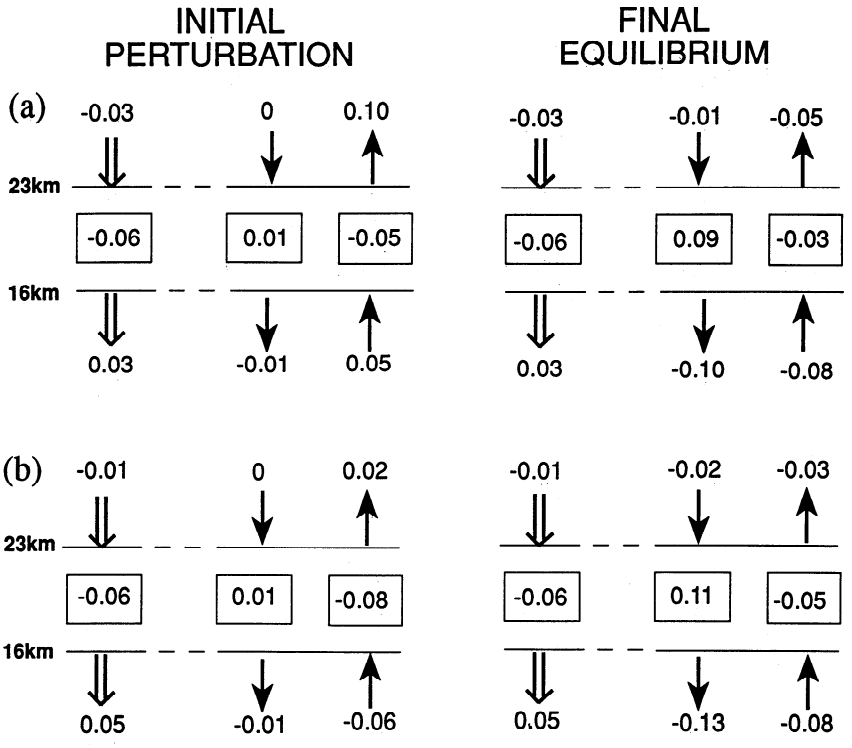

Figure 6. Change in the net solar (open arrow) and upward and downward longwave (solid arrows) fluxes (watts per square meter) at 16 and 23 km and the respective flux convergences (boxed values) within the 16- to 23-km layer corresponding to (a) decrease in stratospheric ozone and (b) stratospheric ozone decrease plus 20% tropospheric ozone increase (see section 5). (Left) The initial perturbations due to changes in the concentrations only and (right) the changes corresponding to the final radiative-convective equilibrium state (see section 5) are represented.

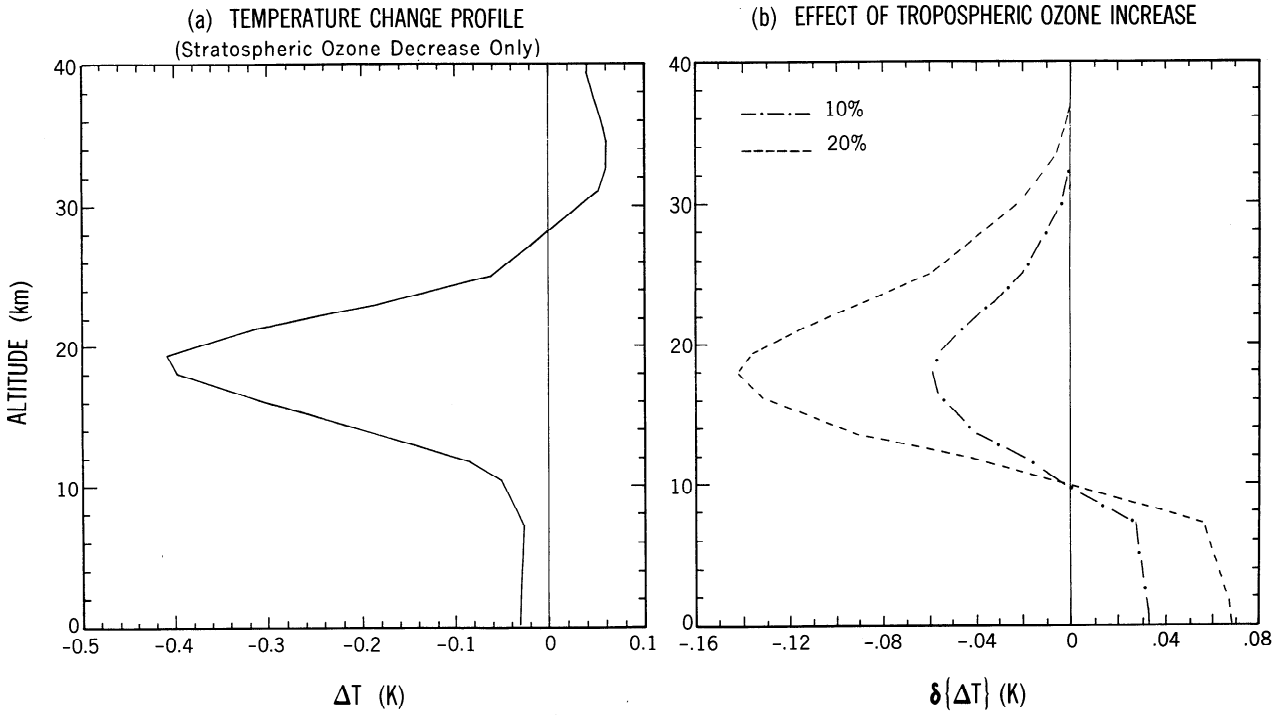

Figure 7. (a) Change in the vertical temperature profile (ΔT) due to a decrease in stratospheric ozone and (b) additional change in stratospheric temperatures $\delta\{\Delta T\}$ due to incorporating a 10% or a 20% increase in tropospheric ozone (see section 5.2).

stratospheric ozone [*Fels et al.*, 1980]. The upward longwave flux shows an increase at 16 km (Figure 6a); this is due to the assumed vertical profile of loss which extends down to 10 km. The reduced infrared absorber amount in the 16- to 23-km layer causes a lesser convergence of the upward longwave flux and a larger upward flux at 23 km. The reduced emission from the 16- to 23-km layer also leads to a decrease in the divergence of the downward longwave flux.

The increase in tropospheric ozone causes an additional contribution to the longwave lower stratospheric cooling rates. There is increased heating in the vicinity of the upper troposphere and a slight increase in the cooling in the lower troposphere, being more noticeable for the 20% tropospheric ozone increase case. Above ~21 km there is a tendency to reduce the heating caused by the stratospheric ozone perturbation. Generally, an increase in tropospheric ozone serves to increase the infrared opacity of the troposphere [*Ramanathan and Dickinson*, 1979], resulting in a significant reduction of the upward longwave radiation in the lower stratosphere (compare Figures 6a and 6b) and causing an enhanced decrease in the lower stratospheric longwave flux convergence (i.e., cooling tendency). The solar flux convergence and the disposition of the downward longwave beam within the lower stratosphere remain unchanged because of the increase in tropospheric ozone. In general, the perturbations occurring in the case of simultaneous stratospheric and tropospheric changes are a sum of the perturbations occurring in the individual cases.

The net (solar plus longwave) radiative heating perturbation (Figure 5c) is the sum of the individual perturbations shown in Figures 5a and 5b. The most significant result is the pronounced cooling in the lower stratosphere due to the additivity of the solar and the infrared tendencies; this is also evident in the net radiative flux divergence inferred from Figure 6b. Figure 5c also illustrates the additivity of the heating in the upper troposphere; this has a smaller magnitude than the change in the lower stratosphere.

5.2. RCM Equilibrium Results

The temperature changes due to perturbations of tropospheric and stratospheric ozone are determined by running the model to a new radiative-convective equilibrium. The calculations were performed for all three atmospheric ozone change cases. Figure 7a shows the change in the vertical temperature profile due to stratospheric ozone loss only. The cooling tendency of the lower stratosphere indicated by the initial perturbations in the heating rates (Figure 5) and fluxes (Figure 6) yield a significant temperature change there, as expected [see *Fels et al.*, 1980] and as also evident in the work of *Miller et al.* [1992]. This result emphasizes the fact that the observed lower stratospheric ozone loss represents a substantial radiative perturbation in a region of the atmosphere where the temperature is strongly sensitive to imbalances in the radiative heating rates. The resulting flux changes at the new equilibrium are displayed in Figure 6 (right) for the stratospheric loss only and with 20% tropospheric ozone increase. As in section 4.2, the comparison of the initial and the final flux dispositions illustrates the effects due to changes in the atmospheric temperatures.

Consider the stratospheric loss only case. Compared to the initial perturbation, there is a further decrease in the divergence of the downward longwave flux, consistent with a cooling of the lower stratosphere and its reduced emission. The latter also causes a decrease of the longwave flux emitted into the troposphere [*Ramaswamy et al.*, 1992], cooling that region as well. The cooling of the troposphere is

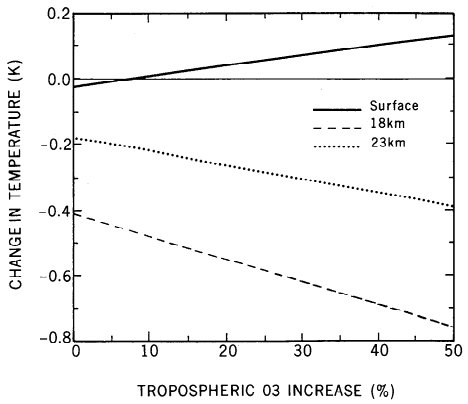

Figure 8. Change in the temperature at the surface, 18 km, and 23 km as a function of tropospheric ozone increase. Stratospheric ozone loss is held fixed (see section 5.2).

accompanied by a reduction of the upwelling flux in the lower stratosphere. Compared to the initial perturbation, there is less of a change in the convergence of this beam within the 16- to 23-km layer. Ultimately, the lower stratospheric radiative equilibrium occurs because of a balance between the changes in the upwelling flux from the troposphere and the emission from the lower stratosphere at its local temperature. The cooling at 18 km is 0.4 K, and the effect is less at higher altitudes (Figure 7a); at 23 km it is ~0.19 K. The magnitude of the cooling below 16 km decreases rapidly with decreasing height, becoming a small uniform value throughout the regions below the upper troposphere (below ~10 km). The tropospheric region affected the most is the upper troposphere, as was pointed out by *Ramanathan and Dickinson* [1979].

Figure 7b shows the additional temperature change introduced by the 10 and 20% increases in tropospheric ozone. There is an enhancement of the temperature decrease in the lower stratosphere, peaking around 19 km. At 18 km this enhancement is 15 and 37% for the two tropospheric ozone cases, respectively; at 23 km the enhancement is 18 and 50%, respectively. The decrease in stratospheric radiative damping times with increasing altitude [*Fels*, 1982; *Kiehl and Solomon*, 1986] causes the effects above the lower stratosphere to be less marked. It can be concluded from Figures 5, 6, and 7b that increases in tropospheric ozone provide an additional mechanism for stratospheric cooling over and above that obtained by a decrease in stratospheric ozone alone. Both of the tropospheric ozone cases emphasize the surface-warming tendency typical of ozone increases in the troposphere [*Ramanathan and Dickinson*, 1979; *Lacis et al.*, 1990; *Schwarzkopf and Ramaswamy*, 1993; *Wang et al.*, 1993]. For the circumstances considered, the surface effects due to the stratospheric ozone loss, with or without tropospheric ozone increases, are small. The overall surface effect of including the tropospheric ozone increases, as specified in this study, is one of warming.

Comparing the left and right panels of Figure 6b, the effects on the longwave and the net solar fluxes due to tropospheric ozone increases follow the same pattern as that in the case of the stratospheric ozone loss. Compared to the initial perturbation, there is a further reduction of the upward longwave flux due to surface-troposphere cooling; there is also a cooling of the lower stratosphere and less of a decrease in the convergence of the upward longwave beam. The lower stratospheric cooling is also accompanied by a further lessening of the divergence in the downward longwave beam. When compared to Figure 6a (right), the additional presence of tropospheric ozone causes an increased cooling of the lower stratosphere such that changes in the flux convergence for the upward beam are slightly greater; also, the change in the divergence of the downward longwave flux is slightly greater.

In a similar manner as above, we have considered the RCE effects due to other values of tropospheric ozone increases. Figure 8 shows the temperature changes obtained at the surface, 18 km, and 23 km with 0–50% increases in tropospheric ozone. The effects at all three heights are nearly linear in ozone change. Table 2 lists the rate of temperature change at the three altitudes. In contrast to the GHGs plus aerosol case (section 4), the surface temperature change is one of an increase, with a 10% global increase exceeding slightly the effect due to the considered stratospheric loss. The temperatures at 18 and 23 km are more sensitive to changes in tropospheric ozone than the surface value. The cooling effect at 18 km due to a 50% increase in tropospheric ozone is ~84% of that induced by the assumed stratospheric loss, while at 23 km the additional cooling effect is 114%. The rate of change of temperature with ozone increase at 23 km is only slightly less sensitive than that at 18 km.

Thus if tropospheric ozone increases of 20% or more have occurred over the past two decades or arise in the future as a consequence of increasing anthropogenic influences, as suggested by model studies [*WMO*, 1992], the changes in lower stratospheric temperatures could become a significant fraction of that due to stratospheric ozone losses. Unfortunately, at present, there are insufficient observations to quantify the global trends in tropospheric ozone [*WMO*, 1992]. If ozone has increased throughout the tropospheric column by large amounts over the past century (so far, the evidence is limited to near-surface observations in Europe [*IPCC*, 1992]), this would have contributed significantly to the cooling of the lower stratosphere over this time period. However, if tropospheric ozone increases are confined to the northern hemisphere midlatitudes, a cooling tendency would occur only in the lower stratosphere of those regions. The influences due to the vertical profile of the ozone changes, as pointed out in several studies [*Wang et al.*, 1980; *Lacis et al.*, 1990; *Schwarzkopf and Ramaswamy*, 1993], cannot be overemphasized. If there were no increases occurring in the upper troposphere (altitude >8 km), the influence shown in Figure 7b would be considerably less. If the stratospheric ozone forcing were more than that considered here, the role

Table 2. Rate of Change of Temperature at the Surface and in the Lower Stratosphere When a Simultaneous Stratospheric Ozone Loss and Tropospheric Ozone Increase Are Considered

	Rate of Change
Surface	0.03 K per 10% increase in tropospheric ozone
18 km	−0.07 K per 10% increase in tropospheric ozone
23 km	−0.04 K per 10% increase in tropospheric ozone

See section 5 and Figure 8.

of a specific tropospheric ozone increase would be diminished.

6. Summary and Discussion

Investigations with a 1-D RCM demonstrate that changes in the concentrations of radiatively active constituents, as known or postulated currently, can contribute to a cooling of the lower stratospheric region. This occurs even if there is no direct initial radiative perturbation in the lower stratosphere. This feature is due essentially to the role of the longwave radiative transfer which couples the lower stratosphere with the troposphere on the one hand and with the middle and the upper stratosphere on the other. The nonlocal radiative exchange process is governed by both the species' concentrations and the temperatures. As is usual in radiative-convective modeling studies, a factor implicit in the numerical results is the parameterization employed to represent the convective process. However, the principal conclusions of this paper regarding the changes in the lower stratosphere are unlikely to be affected by the choice of the convective scheme.

Increases in the well-mixed, nonozone greenhouse gases yield a tropospheric warming and a stratospheric cooling tendency. This leads to changes in the radiative convergence within the lower stratosphere, which causes a temperature decrease there. In the case of an increase in tropospheric aerosols, there is no change initially in the radiative balance of the stratosphere. However, the cooling of the troposphere in response to the increase in the planetary albedo leads to a decrease in the upwelling longwave flux which, in turn, yields a cooling of the lower stratosphere. The establishment of the stratospheric radiative equilibrium in the case of aerosols differs from that for the greenhouse gases, although it leads to the same sign for the temperature change in the lower stratosphere. For simultaneous greenhouse gas and aerosol increases, there is a reduction in the magnitude of the surface-troposphere warming compared to the gas-only case, while in the lower stratosphere the cooling is enhanced. Thus, for example, a tropospheric aerosol optical depth, which completely offsets the greenhouse gas surface-troposphere radiative forcing and results in a null temperature change at the surface, can cause a cooling in the lower stratosphere that is as large as that for the greenhouse gas increases alone.

If there has been an increase in the surface-troposphere radiative forcing by tropospheric aerosols over the past century, it is likely that the lower stratosphere has experienced a cooling tendency beyond that due to the well-mixed greenhouse gases. In view of the many uncertainties associated with the determination of the tropospheric aerosol forcing, it is difficult to gage the extent of the aerosol effect. However, if this forcing is >0.6 W m^{-2}, an important contribution (>37%) by the tropospheric aerosols to the lower stratospheric (18 km) cooling cannot be ruled out. Although this study has considered only one type of aerosol model, the physical mechanism studied here would apply to other tropospheric aerosol models as well wherein the initial perturbation comprises an increase in the planetary albedo. It is worth noting that if cloud microphysics were altered because of the increase in tropospheric aerosols [*Charlson et al.*, 1992], then this indirect aerosol forcing could exert an additional influence on the lower stratospheric temperatures.

In the case of changes in atmospheric ozone the loss of ozone in the lower stratosphere yields a strong decrease of temperature there and a negative surface-troposphere radiative forcing. An increase in tropospheric ozone reduces the upwelling longwave flux at the tropopause, yielding a cooling of the lower stratosphere and a warming tendency for the troposphere. Thus given the observed stratospheric ozone loss, a global increase in tropospheric ozone, even while offsetting the effects of stratospheric loss within the surface-troposphere system, would augment the cooling of the lower stratosphere. Considering, for example, the largest reported increases in tropospheric ozone over the past decade or so (~10–20%), and assuming that the vertical profile of the change extends into the upper troposphere, the induced lower stratospheric cooling effects at 18 km range from 15 to 37% of the effects due to the assumed stratospheric ozone loss. As noted in several studies [e.g., *WMO*, 1986, 1992], the radiative influences would depend on the details of the vertical profile of ozone change and whether or not the tropospheric ozone increases are globally pervasive.

It is now apparent that in addition to being a significant climate change issue in its own right, the cooling of the lower stratosphere due to changes in radiatively active species has important climate implications involving the stratospheric hydrologic cycle [*Toon et al.*, 1986; *Ramaswamy*, 1988] and the chemical and dynamical processes leading to ozone depletion [*Austin et al.*, 1992; *Mahlman et al.*, 1993]. Analysis of the 50- to 100 mbar (~16–20 km) temperatures, using the 1958–1988 radiosonde data, suggests a cooling trend of ~0.3–0.4 K per decade [*Oort and Liu*, 1993]. This represents a substantial change over the considered time period and is unlikely to be due to increases in the well-mixed greenhouse gases alone (see also *Lacis et al.* [1990]). Calculations here show that the entire nonozone greenhouse gas increase between 1850 and 1988 yields a cooling of only ~0.18 K at 18 km. Thus the effect due to the well-mixed greenhouse gases is probably only a small fraction of the observed global lower stratosphere cooling (~1 K) over the past 30 years. This is to be contrasted with the relatively large cooling effects expected due to the well-mixed greenhouse gases in the upper stratosphere [*WMO*, 1986].

The *Miller et al.* [1992] and the present RCM results suggest that the stratospheric ozone loss over the past decade can explain a substantial portion of the observed decadal lower stratospheric cooling. The inhomogeneity of the tropospheric species (aerosols and ozone) and the lack of adequate global measurements make it difficult to assess their respective contributions to the lower stratospheric cooling over the past three decades.

The combined contribution to the lower stratospheric cooling due to global increases in tropospheric ozone and aerosols could well become comparable to or even exceed that due to all the well-mixed greenhouse gases and could even be a significant fraction of that due to the decadal stratospheric ozone loss. If the tropospheric species have increased primarily in the northern hemisphere midlatitudes, then they would have contributed to the lower stratospheric cooling tendency only in those regions. An important conclusion from this study is that since the changes in all the species considered here lead to a cooling tendency for the lower stratosphere, a complete explanation of the temperature trends in the lower stratosphere definitely needs to consider the stratospheric ozone loss, and it requires con-

sideration of the changes in tropospheric ozone and aerosols, besides the usual treatment of the increases in the well-mixed greenhouse gases.

Appendix: Solar Radiative Transfer

The solar radiative transfer scheme employed in the current study is described below. A schematic of the model's vertical structure, consisting of L levels, with 1 being the top of the atmosphere and L the surface, is shown in Figure A1.

We adopt a formulation that combines the delta-Eddington method with an adding scheme similar to that of *Coakley et al.* [1983]. The solar spectrum is divided into 56 intervals; the central wavelength and the bandwidth of each interval are listed in Table A1.

The radiatively active constituents considered are H_2O, CO_2, O_3, CH_4, N_2O, F11, F12, aerosols, and clouds. The optical properties of the constituents in each layer are specified or computed similar to the *Ramaswamy and Kiehl* [1985] (hereinafter referred to as RK) study. For this study the concentrations of trace gases and aerosols are varied, as described in the text. In general, if a layer contains a number of constituents, each of which interacts with the specific solar spectral frequency, the layer single-scattering properties are prescribed as follows:

$$\tau_{\text{ext}}(\text{layer}) = \Sigma\tau_{\text{ext},i} \tag{1}$$

$$\omega(\text{layer}) = \Sigma\tau_{\text{scat},i}/\Sigma\tau_{\text{ext},i} \tag{2}$$

$$g(\text{layer}) = \Sigma\tau_{\text{scat},i}g_i/\Sigma\tau_{\text{scat},i} \tag{3}$$

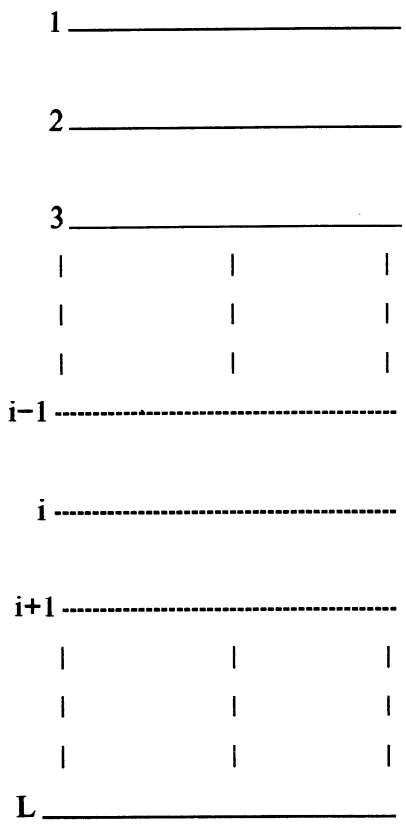

Figure A1. Schematic of the vertical structure of the model.

Table A1. Solar Spectrum Intervals

Interval	Band Center, μm	Bandwidth, μm
1–45*	0.21 (0.01) 0.65	0.01
46	0.66	0.05
47	0.74	0.084
48	0.83	0.096
49	0.95	0.121
50	1.11	0.269
51	1.43	0.298
52	1.62	0.095
53	1.89	0.529
54	2.60	0.791
55	3.30	0.610
56	11.00	99.640†

*The centers of the first 45 bands are 0.01 μm apart.
†The last band accounts for all solar insolation greater than 3.7 μm.

where the sums are over all constituents present in that layer. Next, the delta-Eddington approximation [*Joseph et al.*, 1976] is employed to obtain the reflection and transmission characteristics within each layer and in each spectral interval. Clear and overcast portions of the layers are considered separately. The net reflection and transmission for each layer and within each spectral interval are obtained by weighting the clear and overcast sky by their respective fractions [*Morcrette and Fouquart*, 1986].

With reference to the schematic showing the arrangement of levels, the up and down fluxes can be formulated in terms of the reflection and transmission characteristics of the layers, taking care to distinguish between the properties appropriate for the direct (i.e., unscattered beam) and those appropriate for the diffuse beam, respectively [see *Coakley et al.*, 1983].

$$S_1^{\downarrow} = S_{1d}^{\downarrow} = S_0 \tag{4}$$

$$S_1^{\uparrow} = S_{1d}^{\downarrow}R_1^d + S_2^{\uparrow}T_1^f \tag{5}$$

$$S_2^{\downarrow} = S_{1d}^{\downarrow}t_1^d + S_{1d}^{\downarrow}t_1^f + S_2^{\uparrow}R_1^f = S_{2d}^{\downarrow} + S_{2f}^{\downarrow} \tag{6}$$

$$S_2^{\uparrow} = S_{1d}^{\downarrow}t_1^dR_2^d + S_{2f}^{\downarrow}R_2^f + S_3^{\uparrow}T_2^f \tag{7}$$

$$S_3^{\downarrow} = S_{1d}^{\downarrow}t_1^dt_2^d + S_{1d}^{\downarrow}t_1^dt_2^f + S_{2f}^{\downarrow}T_2^f + S_3^{\uparrow}R_2^f = S_{3d}^{\downarrow} + S_{3f}^{\downarrow} \tag{8}$$

$$S_{i-1}^{\downarrow} = S_{i-1,d}^{\downarrow} + S_{i-1,f}^{\downarrow} \tag{9}$$

$$S_i^{\downarrow} = S_{i,d}^{\downarrow} + S_{i,f}^{\downarrow} \tag{10}$$

$$S_i^{\uparrow} = S_{1d}^{\downarrow}\left(\prod_{k=1}^{i-1} t_k^d\right)R_i^d + S_{i,f}^{\downarrow}R_i^f + S_{i+1}^{\uparrow}T_i^f \tag{11}$$

where the subscript or superscript d and f refer to the direct and diffuse components of the radiation, respectively (see below for more details). S_0 is the solar spectral irradiance at the top and follows *Labs and Neckel* [1970]. Further,

$$t_i^d = \exp\,(-\tau_i/\mu_0) \tag{12}$$

$$S_{i,d}^{\downarrow} = S_{1d}^{\downarrow}\left(\prod_{k=1}^{i-1} t_k^d\right) \tag{13}$$

$$S_{i,f}^{\downarrow} = S_{i-1,d}^{\downarrow}t_{i-1}^f + S_i^{\uparrow}R_{i-1}^f + S_{i-1,f}^{\downarrow}T_{i-1}^f \tag{14}$$

with $S_{1f}^{\downarrow} = 0$, and

$$t_i^f = T_i^d - \exp(-\tau_i/\mu_0) = T_i^d - t_i^d \quad (15)$$

R and T are the reflection and transmission functions of layers, with the superscripts denoting whether they are with respect to direct (d) or diffuse (f) beams incident on the layer. Radiation scattered at least once is considered diffuse, and the diffuse beam is assumed to be isotropic. T_i^d denotes the total transmissivity by a layer to direct incident radiation, with t_i^d being the component transmitted as direct (i.e., unscattered portion) and t_i^f being the component transmitted as diffuse (i.e., scattered at least once); μ_0 is the cosine of the incident solar zenith angle. T_i^f is the transmissivity of the layer to diffuse incident radiation. The subscripts d and f on the downward ($S^{\downarrow}$) fluxes indicate whether they represent the direct or the diffuse beam, respectively. The upward flux ($S^{\uparrow}$) is always diffuse.

Equations (4)–(11) are rearranged in the form of a pentadiagonal matrix which is then inverted to obtain the up and down fluxes. This procedure is repeated for each of the 56 spectral intervals.

Acknowledgments. The authors thank K. Hamilton and M. D. Schwarzkopf for their comments on the paper. M.M.B.'s work was supported through a summer undergraduate internship with the Atmospheric and Oceanic Sciences Program of Princeton University.

References

Austin, J., N. Butchart, and K. P. Shine, Probability of an Arctic ozone hole in a doubled CO_2 climate, *Nature*, *360*, 221–225, 1992.

Charlson, R. J., J. Langner, H. Rodhe, C. B. Leovy, and S. G. Warren, Perturbation of the northern hemisphere radiative balance by backscattering from anthropogenic sulfate aerosols, *Tellus*, *Ser. A-B*, *43*(4), 152–163, 1991.

Charlson, R. J., S. E. Schwartz, J. M. Hales, R. D. Cess, J. A. Coakley, J. E. Hansen, and D. J. Hoffman, Climate forcing by anthropogenic aerosols, *Science*, *255*, 423–430, 1992.

Coakley, J. A., R. D. Cess, and F. B. Yurevich, The effect of tropospheric aerosols on the Earth's radiation budget: A parameterization for climate models, *J. Atmos. Sci.*, *40*, 116–138, 1983.

Fels, S. B., A parameterization of scale-dependent radiative damping rates in the middle atmosphere, *J. Atmos. Sci.*, *39*, 1141–1152, 1982.

Fels, S. B., J. D. Mahlman, M. D. Schwarzkopf, and R. W. Sinclair, Stratospheric sensitivity to perturbations in ozone and carbon dioxide: Radiative and dynamical response, *J. Atmos. Sci.*, *37*, 2265–2297, 1980.

Hansen, J. E., and A. A. Lacis, Sun and dust versus greenhouse gases: An assessment of their relative roles in global climate change, *Nature*, *346*, 713–719, 1990.

Intergovernmental Panel on Climate Change (IPCC), *Climate Change: The Scientific Assessment*, edited by J. T. Houghton, B. Callander, and S. K. Varney, 200 pp., Cambridge University Press, New York, 1992.

Joseph, J. H., W. J. Wiscombe, and J. A. Weinman, The delta-Eddington approximation for radiative flux transfer, *J. Atmos. Sci.*, *33*, 2452–2459, 1976.

Kiehl, J. T., and B. P. Briegleb, The relative roles of sulfate aerosols and greenhouse gases in climate forcing, *Science*, *260*, 311–314, 1993.

Kiehl, J. T., and S. Solomon, On the radiative balance of the stratosphere, *J. Atmos. Sci.*, *43*, 1525–1534, 1986.

Labs, D., and H. Neckel, Transformation of the absolute solar radiation data into the international temperature scale of 1968, *Sol. Phys.*, *15*, 79–87, 1970.

Lacis, A. A., D. J. Wuebbles, and J. A. Logan, Radiative forcing of climate by changes in the vertical distribution of ozone, *J. Geophys. Res.*, *95*, 9971–9981, 1990.

Mahlman, J. D., J. P. Pinto, and L. J. Umscheid, Transport, radiative and dynamical effects of the Antarctic ozone hole: A GFDL "SKYHI" model experiment, *J. Atmos. Sci.*, *51*, 489–508, 1993.

Manabe, S., and F. Moller, On radiative equilibrium and heat balance of the atmosphere, *Mon. Weather Rev.*, *89*, 503–532, 1961.

Manabe, S., and R. T. Wetherald, Thermal equilibrium of the atmosphere with a given distribution of relative humidity, *J. Atmos. Sci.*, *24*, 241–259, 1967.

McClatchey, R. A., R. W. Fenn, J. E. A. Selby, F. E. Volz, and J. S. Garing, Optical properties of the atmosphere, 3rd ed., *Rep. AFCRL-72-0497*, Air Force Cambridge Res. Lab., Bedford, Mass., 1972.

Miller, A. J., R. M. Nagatani, G. C. Tiao, X. F. Niu, G. C. Reinsel, D. Wuebbles, and K. Grant, Comparisons of observed ozone and temperature trends in the lower stratosphere, *Geophys. Res. Lett.*, *19*, 929–932, 1992.

Morcrette, J. J., and Y. Fouquart, The overlapping of cloud layers in shortwave radiation parameterizations, *J. Atmos. Sci.*, *43*, 321–328, 1986.

Oort, A. H., and H. Liu, Upper air temperature trends over the globe, 1958–1989, *J. Clim.*, *6*, 292–307, 1993.

Penner, J., R. E. Dickinson, and C. A. O'Neill, Effects of aerosols from biomass burning on the global radiation budget, *Science*, *256*, 1432–1434, 1992.

Ramanathan, V., The role of ocean-atmosphere interactions in the CO_2 climate problem, *J. Atmos. Sci.*, *38*, 918–930, 1981.

Ramanathan, V., and R. E. Dickinson, The role of stratospheric ozone in the zonal and seasonal radiative energy balance of the Earth-troposphere system, *J. Atmos. Sci.*, *36*, 1084–1104, 1979.

Ramanathan, V., R. J. Cicerone, H. B. Singh, and J. T. Kiehl, Trace gas trends and their potential role in climate change, *J. Geophys. Res.*, *90*, 5547–5566, 1985.

Ramaswamy, V., Dehydration mechanism in the Antarctic winter stratosphere, *Geophys. Res. Lett.*, *15*, 863–866, 1988.

Ramaswamy, V., and J. T. Kiehl, Sensitivities of the radiative forcing due to large loadings of smoke and dust aerosols, *J. Geophys. Res.*, *90*, 5597–5613, 1985.

Ramaswamy, V., M. D. Schwarzkopf, and K. P. Shine, Radiative forcing of climate from halocarbon-induced global stratospheric ozone loss, *Nature*, *355*, 810–812, 1992.

Rodgers, C. D., and C. D. Walshaw, The computation of infrared cooling rates in planetary atmospheres, *Q. J. R. Meteorol. Soc.*, *92*, 67–92, 1966.

Schwarzkopf, M. D., and S. B. Fels, The simplified exchange method revisited: An accurate, rapid method for computation of infrared cooling rates and fluxes, *J. Geophys. Res.*, *96*, 9075–9096, 1991.

Schwarzkopf, M. D., and V. Ramaswamy, Ozone changes in the 1980s: Dependence on the altitude profile of ozone change, *Geophys. Res. Lett.*, *20*, 205–208, 1993.

Shettle, E. P., and R. W. Fenn, Models for the aerosols of the lower atmosphere and the effects of humidity variations on their optical properties, *Rep. AFGL-TR-79-0214*, 94 pp., Air Force Geophys. Lab., Bedford, Mass., 1979.

Toon, O. B., P. Hammill, R. P. Turco, and J. P. Pinto, Condensation of HNO_3 and HCl in the winter polar stratosphere, *Geophys. Res. Lett.*, *13*, 1284–1287, 1986.

Wang, W.-C., J. P. Pinto, and Y. L. Yung, Climate effects due to halogenated compounds in the Earth's atmosphere, *J. Atmos. Sci.*, *37*, 333–338, 1980.

Wang, W.-C., Y.-C. Zhuang, and R. D. Bojkov, Climate implications of observed changes in ozone vertical distributions at middle and high latitudes of the northern hemisphere, *Geophys. Res. Lett.*, *20*, 1567–1570, 1993.

World Meteorological Organization (WMO), Atmospheric Ozone 1985, *Rep. 16*, Global Ozone Res. and Monit. Proj., Geneva, 1986.

World Meteorological Organization (WMO), Scientific Assessment of Ozone Depletion, *Rep. 25*, Global Ozone Res. and Monit. Proj., Geneva, 1992.

M. M. Bowen and V. Ramaswamy, Atmospheric and Oceanic Sciences Program, Princeton University, Princeton, NJ 08542.

(Received June 29, 1993; revised May 5, 1994; accepted May 13, 1994.)